AD_____

CONTRACT NUMBER DAMD17-96-C-6086

TITLE: Thin Film CdZnTe Detector Arrays for Digital Mammography

PRINCIPAL INVESTIGATOR: Harvey B. Serreze, Ph.D.

CONTRACTING ORGANIZATION: Spire Corporation
Bedford, Massachusetts 01730-2396

REPORT DATE: December 1998

TYPE OF REPORT: Annual

PREPARED FOR: U.S. Army Medical Research and Materiel Command
Fort Detrick, Maryland 21702-5012

REPORT DOCUMENTATION PAGE

Form Approved OMB No. 0704-0188

1. AGENCY USE ONLY *(Leave blank)*	2. REPORT DATE	3. REPORT TYPE AND DATES COVERED
	December 1996	Annual (26 Sep 97 - 25 Sep 98)

4. TITLE AND SUBTITLE

Thin Film CdZnTe Detector Arrays for Digital Mammography

5. FUNDING NUMBERS

DAMD-17-96-C-6086

6. AUTHOR(S)

Harvey B. Serreze, Ph.D.

7. PERFORMING ORGANIZATION NAME(S) AND ADDRESS(ES)

Spire Corpoation
Bedford MA 01730-2396

8. PERFORMING ORGANIZATION REPORT NUMBER

10178

9. SPONSORING/MONITORING AGENCY NAME(S) AND ADDRESS(ES)

U.S. Army Medical Research and Materiel Command
Attn: MCMR-RMI-S
504 Scott Street
Fort Detrick, MD 21702-5012

10. SPONSORING/MONITORING AGENCY REPORT NUMBER

11. SUPPLEMENTARY NOTES

12a. DISTRIBUTION/AVAILABILITY STATEMENT

12b. DISTRIBUTION CODE

13. ABSTRACT *(Maximum 200 words)*

The objective of this program has been to develop large-area, flat-panel detectors for digital mammography using CdTe or CdZnTe deposited directly on thin-film transistor (TFT) active matrix arrays for image readout. CdTe and CdZnTe have the potential to meet the requirements for digital mammography because they have high X-ray absorption, large bandgap, and high resistivity. Activities during the second year were directed principally toward the optimization of physical and electrical properties of MOCVD-deposited CdTe and CdZnTe, and improved understanding of the CdS/Cd(Zn)Te heterojunctions used to reduce the leakage currents. By planarizing the growth susceptor, improved film morphology was realized. Studies of growth rate vs. temperature showed that reasonable growth rates could be obtained at temperatures as low as 250°C using readily-available precursors. Films of CdZnTe were obtained by incorporation of a Zn precursor into the growth chamber. Electrical characterization of the films continued; however, leakage currents are still too high in spite of a CdS-based heterostructure. It is not certain whether these currents are due to film purity or grain boundary effects, but it is imperative that this problem be solved before the program embarks on deposition of films onto active device structures. Film improvement will therefore be the primary focus for the coming year.

14. SUBJECT TERMS

CdTe, CdZnTe, array, mammography, MOCVD, TFT, heterojunction

15. NUMBER OF PAGES

35

16. PRICE CODE

17. SECURITY CLASSIFICATION OF REPORT	18. SECURITY CLASSIFICATION OF THIS PAGE	19. SECURITY CLASSIFICATION OF ABSTRACT	20. LIMITATION OF ABSTRACT
Unclassified	Unclassified	Unclassified	Unlimited

FOREWORD

Opinions, interpretations, conclusions, and recommendations are those of the author and are not necessarily endorsed by the U.S. Army.

X Where copyrighted material is quoted, permission has been obtained to use such material.

X Where material from documents designated for limited distribution is quoted, permission has been obtained to use the material.

X Citations of commercial organizations and trade names in this report do not constitute an official Department of Army endorsement or approval of the products or services of these organizations.

N/A In conducting research using animals, the investigator(s) adhered to the "Guide for the Care and Use of Laboratory Animals," prepared by the Committee on Care and Use of Laboratory Animals of the Institute of Laboratory Resources, National Research Council (NIH Publication No. 86-23, Revised 1985).

✓ For the protection of human subjects, the investigator(s) adhered to policies of applicable Federal Law 45 CFR 46.

N/A In conducting research utilizing recombinant DNA technology, the investigator(s) adhered to current guidelines promulgated by the National Institute of Health.

N/A In the conduct of research utilizing recombinant DNA, the investigator(s) adhered to the NIH Guidelines for Research Involving Recombinant DNA Molecules.

N/A In the conduct of research involving hazardous organisms, the investigator(s) adhered to the CDC-NIH Guide for Biosafety in Microbiological and Biomedical Laboratories.

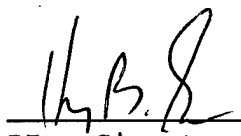

PI - Signature

12/11/98

Date

TABLE OF CONTENTS

LIST OF FIGURES

LIST OF TABLES

5. INTRODUCTION

Early detection of breast cancer can reduce mortality from the disease. X-ray screen-film mammography is well entrenched for early detection, because it offers greater sensitivity and specificity for breast tumors than any other noninvasive diagnostic technique currently available in hospitals. Though screen-film image receptors perform well, they have several limitations, including poor contrast and resolution, increased noise at high spatial frequencies, and low quantum efficiency. Poor contrast occurs due to the inherent sigmoidal response curve of film to light; this limits contrast in both the thin and dense portions of the breast. Due to the spread of light before it escapes, the screen degrades resolution, and has a limited quantum efficiency because its thickness must be limited to minimize image blur. Noise arises from granularity in the film emulsion, variations in the amount of light emitted per interacting X-ray, and from X-rays escaping through the screen. An anti-scatter grid is used to prevent degradation in contrast and signal-to-noise ratio (SNR) from X-rays scattered in the breast. This necessitates a 2.5 to 3 times increase in dose to the breast because the grid removes both scattered and primary X-rays.[1-3]

Many of the limitations of screen-film mammography could be effectively overcome with a digital mammography imaging system in which image acquisition, display, and storage are performed independently, allowing optimization of each step. The challenges in creating a digital mammography system with improved performance are related primarily to detector design. Characteristics of the detector should include efficient absorption of the incident radiation beam, linear response over a wide range of incident radiation intensity, low intrinsic noise, spatial resolution on the order of 50 μm, and the ability to accommodate at least an 18 x 24 cm field size.

Cadmium telluride (CdTe) and cadmium zinc telluride (CdZnTe or "CZT")-based detectors have the potential to meet the above requirements because they offer direct detection, high detection efficiency, high signal-to-noise ratio, and large dynamic range. CdTe and CdZnTe have many attractive properties including high absorption in the keV to MeV energy range, large bandgap, and high resistivity.

Several groups are currently investigating bulk CdZnTe detectors and arrays for imaging applications in nuclear medicine.[4-8] By alloying 10 to 20% Zn in CdTe, resistivity is increased from about 10^9 to 10^{11} ohm-cm and leakage current is decreased by virtue of an increase in bandgap from 1.45 eV to 1.7 eV. Barber *et al.*[4] have developed CdZnTe detector arrays for nuclear medicine. Singh *et al.*[5] evaluated CdZnTe detectors for electronically collimated single photon emission computed tomography (SPECT) to replace cryogenically cooled Ge detectors. These and other work have confirmed the high performance of CdTe and CdZnTe bulk detectors which are generally used for high energy applications. Room temperature detectors made of bulk crystalline CdTe and CdZnTe having low leakage current and high energy resolution are commercially available from various companies including Spire.

While relatively limited work has been reported on thin film CdTe or CdZnTe X-ray detectors, results to date strongly support the potential of thin-film CdTe or CdZnTe for X-ray imaging. Efforts to investigate CdTe thin films for X-ray detection include the following: 1) A CdTe photoconductor-array X-ray detector grown by molecular beam epitaxy (MBE) on a Si substrate by Yoo *et al.* and irradiated with a 50 μm wide synchrotron beam showed excellent spatial resolution, exhibited linear response in the 12 to 15 keV energy range, and showed a temporal response as fast as 20 ps.[9] 2) A group from France investigating polycrystalline MOCVD-grown CdTe thin films to detect fast X-ray pulses produced by laser-induced plasmas demonstrated picosecond response.[10] 3) A Japanese group working on an X-ray imaging camera employing thin film CdTe/CdS heterojunction photodiodes deposited by rf sputtering showed high X-ray response.[11] The group then went on to develop a one-inch X-ray imaging camera tube based upon this heterojunction; the camera had three times larger responsivity to X-rays than a conventional PbO (lead oxide) X-ray tube. The resolution of their device was greater than 25 lines/mm.

Based on the promise and demonstrated success of CdTe and CdZnTe, the application of these materials to digital mammography appears to be a logical extension of the technology. Spire Corporation has had nearly fifteen years experience with high quality, semiconductor thin film materials made by metalorganic chemical vapor deposition (MOCVD), some of this work directly with CdTe and CdZnTe for other electronic applications (primarily infrared detector substrates). For the past two years we have been investigating these materials for future use in digital mammography applications. Spire also continues to be involved, both commercially and in research, with high energy detectors using bulk CdZnTe.

6. PROGRAM OVERVIEW

The objective of the four-year program addressed in this Second Annual Report is to develop a large-area, flat-panel solid-state X-ray detector for digital mammography using thin-film CdTe or CdZnTe deposited directly on a thin-film transistor (TFT) active matrix array for image readout. To demonstrate this concept, we have proposed to fabricate and test a prototype 1024 x 1024 integrated detector array having 50 μm x 50 μm pixels. The array will employ a high resistivity CdTe or CdZnTe semiconductor layer to convert the incident X-rays to electron-hole pairs, and the resulting charge image will be read out digitally by a pixellated CdSe TFT array. The detector concept is illustrated in Figure 1.

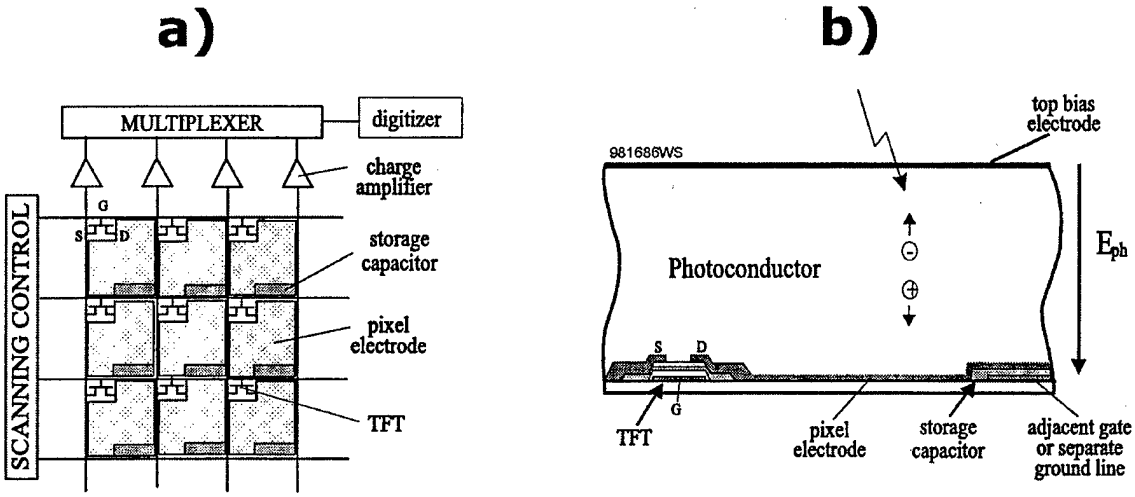

Figure 1 Diagram of the proposed detector concept.

We had planned to develop this detector array in three phases. The first phase was to develop the necessary CdTe or CdZnTe thin films. As part of the effort, we would design and fabricate CdTe or CdZnTe passive matrix detector test arrays with pixel sizes varying from 50 μm to 500 μm on various substrates including glass, gallium arsenide (GaAs), and silicon (Si). Passive matrix detector arrays are relatively simple to fabricate and do not require extensive electronics for testing. These arrays would allow us to measure detection efficiency, signal linearity, pixel size effects, optimum operating voltage, leakage current, and pixel-to-pixel uniformity. The results of these experiments would be used to optimize deposition conditions and detector design parameters. Spire would deposit the films and would design and fabricate the passive matrix detector arrays. Professor John Rowlands from the University of Toronto would characterize the arrays and perform theoretical calculations to determine parameters such as signal level, detection efficiency, X-ray quantum noise, and inherent spatial resolution.

In the second phase we had proposed to integrate prototype CdTe or CdZnTe detector arrays with Si multiplexers. Optimized deposition conditions for the CdZnTe films determined in the first stage were to be employed. A Si multiplexer was selected because of its lower cost than the CdSe TFT arrays ultimately to be used. We had planned to employ a 128 x 128 matrix array with 60 μm center-to-center element spacing. Spire was to deposit the thin films on the Si multiplexers, and the University of Toronto was to test these arrays.

In phase three, once the detector fabrication process and the electronics are determined, we had planned to develop a 5 cm x 5 cm prototype self-scanned detector array by integrating thin-film CdTe or CdZnTe detectors with a CdSe TFT array. The purpose of developing a 5 cm x 5 cm prototype was twofold: first, these arrays would be useful for strerotaxic breast biopsy, and second, they would be a first stage demonstration of an 18 x 24 cm large-area detector suitable for digital mammography. The prototype was to be developed jointly with Professor Rowlands and Litton Systems Canada, Ltd., the only North American vendor of CdSe TFTs, and was planned to have 1024 x 1024 50-μm pixel elements. Spire would deposit the CdZnTe detectors on these TFT arrays. Professor Rowlands, in collaboration with Spire, would assemble and characterize the detector arrays. Finally, phantom images using these arrays were to be obtained to demonstrate the usefulness of this approach for digital mammography.

During the first year, we begun initial experiments to deposit and examine CdTe and CdZnTe thin films that would be suitable for X-ray detection. CdTe and CdZnTe thin films were deposited by thermal evaporation and metalorganic chemical vapor deposition (MOCVD) onto a variety of substrates including ITO (indium tin oxide)-coated glass, CdS/ITO-coated glass, GaAs, and plain glass. Samples were characterized for morphology, crystal quality, thickness, and electrical properties. Results indicated that films deposited by MOCVD possessed properties superior to those of evaporated films. Consequently, emphasis was directed toward the MOCVD materials. However, further experiments revealed that even the best MOCVD films still did not possess sufficiently high resistivity to give the necessary low leakage current values required. This problem was partially solved by modifying our original device design to include a CdS/Cd(Zn)Te heterojunction blocking-contact configuration similar to a design we had developed previously. The consequence of these unanticipated problems was that many of the planned materials optimization and array design activities were either not completed or not started according to the original schedule.

During the second year, experiments focused on continuing optimization of the CdTe and CdZnTe films grown by MOCVD. Because of the importance of the material properties in determining the operating characteristics of the final X-ray detector array, it has been necessary to redirect efforts in order to properly address this very crucial issue. Consequently, many of the original tasks focusing on device-related issues (such as preliminary arrays on Si multiplexer arrays) will have to be either delayed or canceled. Until material properties are brought to the proper level, it is premature to go to the next steps in the development process.

7. SUMMARY OF SECOND YEAR RESULTS

Experimental activities during the second year focused on improving the basic material and device results obtained during the first year. Efforts were directed principally in two areas: 1) optimization of physical and electrical properties of MOCVD-deposited CdTe and CdZnTe, and 2) improved understanding of the operation of CdS/Cd(Zn)Te heterojunctions to reduce the leakage currents. Highlights of these activities are presented below.

In order to make the detector array shown in Figure 1, four principal criteria are required for the thin-film Cd(Zn)Te materials. First, the films should be sufficiently thick to absorb the incident X-ray beam. Second, the film deposition process must be compatible with the underlying TFT array in terms of deposition temperature, processing steps, etc. Third, the electrical properties of the Cd(Zn)Te films must be suitable to assure adequate collection of the X-ray generated carriers without the occurrence of undesired phenomena such as slow response speed, afterglow, *etc.* Finally, in order to guarantee a process that is practical, the deposition method must be sufficiently low cost which translates into issues such as cost of the raw materials, deposition rate, yield, *etc.*

The first and second issues, namely film thickness and deposition temperature, are closely interrelated and have needed to be to examined together. One reason that CdSe TFTs were selected over other candidates such as amorphous silicon (a-Si) is the fact that CdSe TFTs can withstand higher temperatures (typically 350°C) compared to a-Si (which is limited to about 250°C). This higher temperature allows greater flexibility in selecting a thin-film deposition process that produces material with good properties while maintaining reasonable deposition rate. These factors prompted a series of MOCVD growth runs to examine the effects of growth temperature on film properties and growth rate. Some of these experiments are still continuing due to the large number of independent variables which include choice of metalorganic source material, Zn composition, and MOCVD growth parameters (*e.g.*, VI/II ratio, flow rates, reactor geometry, *etc.*).

Shown in Table 1 are results of a series of CdTe runs deposited on single-crystal GaAs substrates designed to examine deposition rate and film properties (principally, physical quality). These runs were all performed under similar conditions (pressure, VI/II ratio, absolute flow rates, *etc.*). It is apparent from these results that acceptable growth rates (>8 μm/hr) can occur under all conditions within the boundaries of these experiments. Film quality as determined by both physical appearance and X-ray crystallographic analysis (FWHM of X-ray peak) was also good.

Table 1 **Summary of a series of CdTe MOCVD runs conducted at 500 torr pressure, VI/II=2.9, using dimethylcadmium (DMCd) and dimethyltellurium (DMTe). All films were deposited on semi-insulating GaAs substrates (2° off 100 orientation).**

Run No. (M4-)	Growth Temp. (°C)	Time (min.)	Thickness (μm)	Rate (μm /hr)	X-ray FWHM (arc sec)	Physical Appearance
4497	380	30	4.3	8.6	288	slight haze
4493	400	30	5.6	11.3	144	good
4495	420	30	7.0	14.0	90	excellent
4500	440	30	7.2	14.3	180	excellent

It is known that film deposition rate and minimum growth temperature also depend on the particular MOCVD starting materials (precursors) that are used. For the runs indicated in Table 1, the tellurium source was DMTe (dimethyl tellurium). Other sources have been developed, and selected ones are listed in Table 2. DMTe has been used for most of our experiments because of its availability, purity, and relative low cost. However, it may not be the best choice for low-temperature growth of tellurides. A tellurium precursor with better low-temperature growth potential is diallyl telluride (DATe) which is also listed in Table 2. The main disadvantage of DATe is its higher cost ($48/g) which is due primarily to low demand. CdTe has been successfully grown using DATe for HgCdTe infrared sensor substrate applications at temperatures as low as 240°C, but with relatively slow growth rates (only 0.6 μm/hr).[13] While MOCVD growth of CdTe has been demonstrated at temperatures as low as 220°C using ditertiarybutyl tellurium (DTBTe)[14], DTBTe is currently not commercially available.

Table 2 **Properties of selected tellurium precursors (Ref. 12).**

Precursor	Abbreviation	Vapor Pressure (torr @ °C)	Demonstrated Growth Temperature	Cost (in 500g quantity)
Dimethyl tellurium	DMTe	51.9 @ 25	500	$33/g
Diethyl tellurium	DETe	9.3 @ 25	450	Not commercially available
Diisopropyl tellurium	DIPTe	5.6 @ 30	350	Not commercially available
Diallyl tellurium	DATe	3.3 @ 40	240 (Ref. 13)	$48/g
Ditertiarybutyl tellurium	DTBTe	4.3 @ 50	220 (Ref. 14)	Not commercially available

Shown in Figure 2 are data showing MOCVD growth rate of CdTe on glass, ITO-coated glass, or CdS/ITO-coated glass substrates as a function of deposition temperature. Some of these data are from this program, some are from an ongoing related commercial program at Spire. A variety of growth conditions are included (e.g., specific precursors, VI/II ratio, pressure, absolute flow rates, *etc.*). The important points, however, are: 1) the growth rate increases with temperature, and 2) slow, but reasonable, growth rates are possible at temperatures as low as 250°C. These have important ramifications for this program, namely that reasonable growth can be expected in the 350°C temperature range which is that needed for deposition onto CdSe TFT arrays.

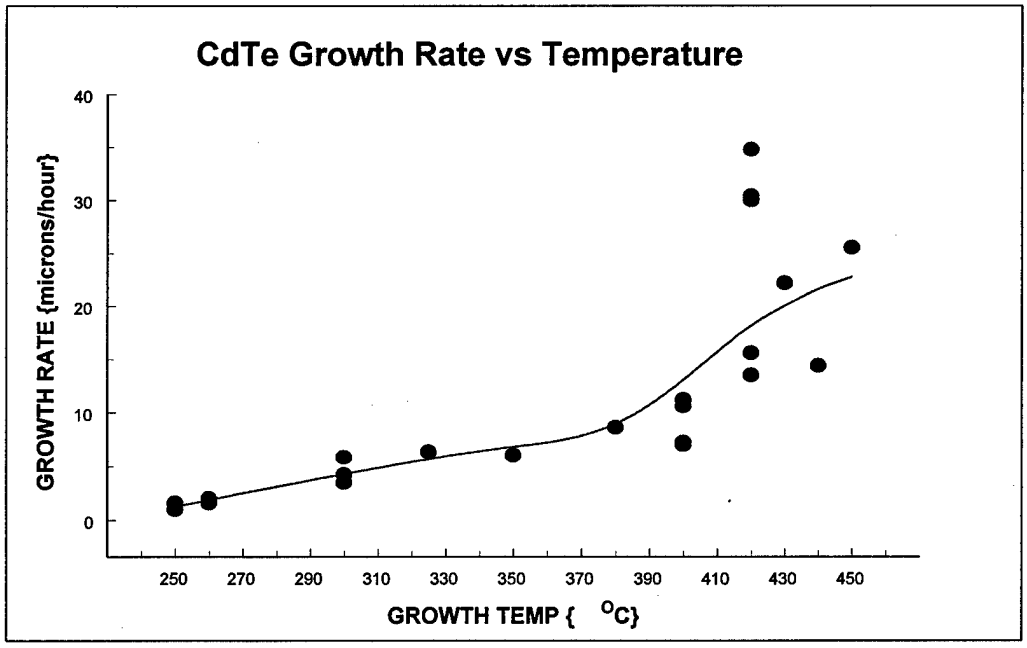

Figure 2 **Growth rate for MOCVD-deposited CdTe as a function of temperature.**

Another important requirement for the deposited films is that they possess good surface morphology and smooth surfaces, particularly for thicker films (>100 μm). Formation of particulates within the growth chamber and their falling onto the substrate during growth can be especially problematic. Early growth runs often suffered from this problem as demonstrated in Figure 3. This profilometer plot shows a surface scan for a CZT thin film (approximately 5 μm thick) deposited on an ITO-coated glass substrate; surface features approximately equal to the film thickness are apparent.

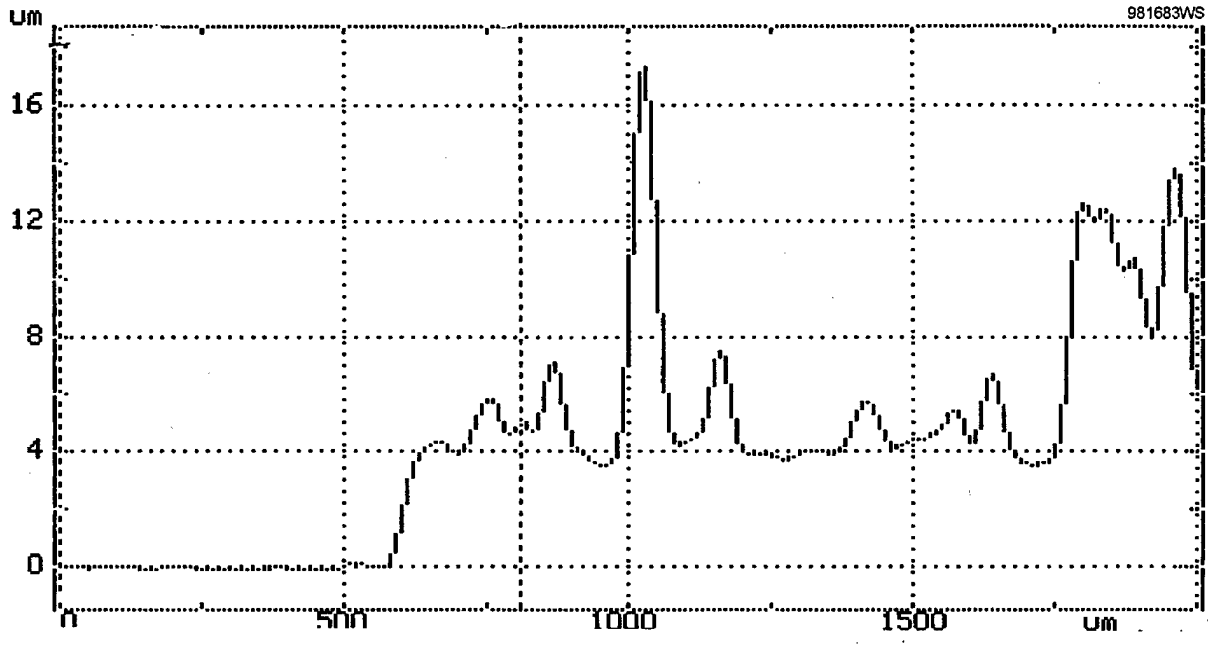

Figure 3 **Profilometer plot of a CZT film (M4-4549) deposited on an ITO-coated glass substrate using a flat susceptor.**

During growth of films such as that in Figure 3, the glass, ITO-coated glass , or CdS/ITO-coated glass substrates (typically 1-2 mm thick) have sat horizontally on an rf-heated, flat graphite susceptor. Since the injected gases flow vertically downward, the opportunity exists for small eddy currents to form near the substrate edges which can lead to CdTe particle formation and subsequent deposition onto the substrate. If these deposits form early in the growth process, they can act as nuclei for further growth and thus lead to larger particles which result in a very rough surface. To solve this problem, we replaced the flat susceptor with a "pocketed" susceptor with recesses machined into the susceptor top surface that were the same size, shape, and depth (thickness) as the glass substrates, thus resulting in a growth surface which was essentially planar with no features. Results of growth of a similar thickness film using the new susceptor appear in Figure 4. Compared to the film shown in the previous figure, this film is clearly superior in its surface smoothness.

Materials studied during this program include both CdTe and CdZnTe (CZT). CZT has the advantage that the addition of Zn to CdTe raises the bandgap and increases the resistivity. However, the X-ray absorption is slightly decreased because Zn (Z=30) has a smaller atomic number, Z, than Cd (Z=48). The net result of these counteracting effects is that there is an optimum Zn concentration which is usually in the 10 to 20 mole percent range.

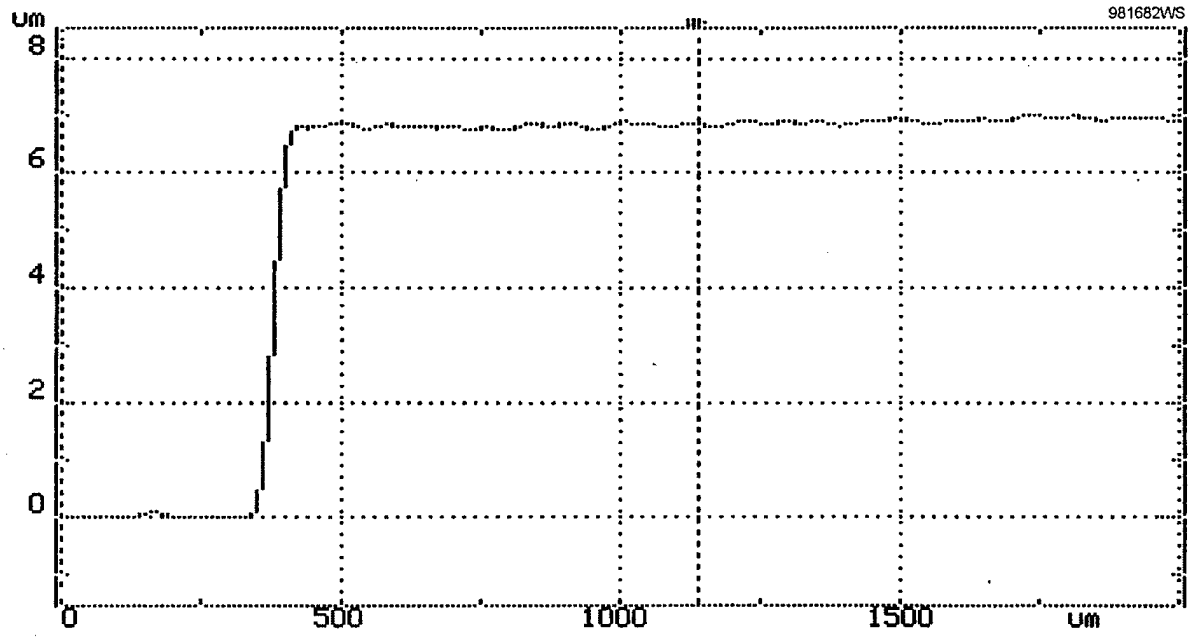

Figure 4 **Profilometer plot of a CZT film (M4-4632) grown using a "pocketed" susceptor.**

Summarized in Table 3 is a series of runs performed to study the effects of Zn incorporation in CZT films. All films were deposited on ITO-coated glass substrates under the conditions noted in the Table, and Zn concentration of the $Cd_{1-x}Zn_xTe$ was determined from optical transmission measurements to determine the bandgap, E_g, which is uniquely related to Zn concentration, x, through the empirical relationship

$$E_g(x) = 1.51 + (0.606)x + (0.139)x^2. \quad (1)$$

An example of an optical transmission experiment result is shown in Figure 5. The bandgap is estimated by extrapolating the linear region of the band edge to the ordinate.

Table 3 **Summary of MOCVD experiments aimed at studying Zn incorporation. Zn concentration was determined from optical transmission measurements.**

Run No.	Growth Temp (C)	DMCd Flow (sccm)	DEZn Flow (sccm)	Cd/Zn Ratio	DMTe Flow (sccm)	VI/II Ratio	Zn conc.
4533	420	155	75	2.07	375	2.92	0.00
4536	420	100	100	1.00	290	2.97	0.00
4537	420	75	100	0.75	240	2.98	0.00
4542	420	60	150	0.40	145	1.71	0.08
4541	420	40	100	0.40	100	1.77	0.28
4545	430	40	100	0.40	100	1.77	0.28
4544	440	40	100	0.40	100	1.77	0.40
4539	420	30	100	0.30	100	2.02	0.40
4540	420	20	100	0.20	120	2.81	0.57
4535	420	0	100	0.00	87	3.01	1.00

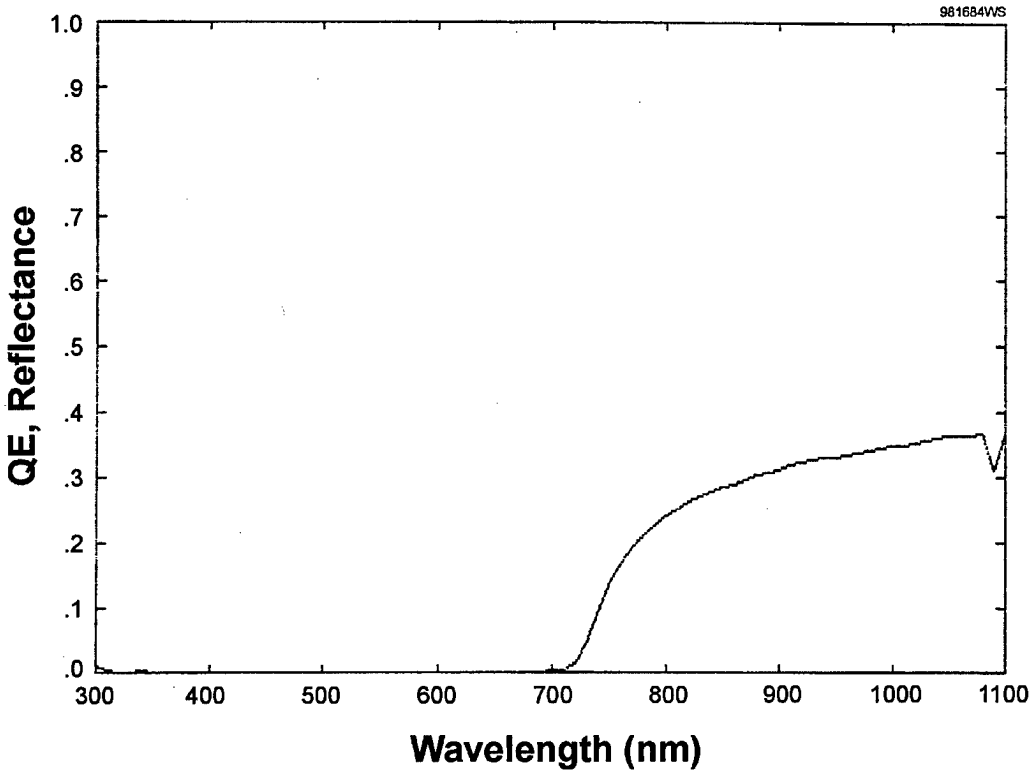

Figure 5 **Example of an optical transmission characteristic of an MOCVD-deposited CdZnTe film (Run M4-4541). For this film, the estimated band edge is 730 nm which corresponds to a bandgap of 1.70 eV, and, through Equation (1), to an x-value of 0.28.**

Ultimately, the goal is to be able to predict the value of x from the anticipated MOCVD growth parameters. Results of an attempt to attribute x to the Zn-to-Cd ratio based on the data in Table 3 is shown in Figure 6. This figure suggests a monotonic dependence of x on Zn-to-Cd ratio, but this data is for growth in the 420 to 440°C temperature range only. Growth at other temperatures such as the lower ones ultimately required to deposit films on CdSe TFT arrays will undoubtedly change these results, and this issue will continue to be the focus of future experiments.

Finally, a preliminary CZT sample on a CdS/ITO-coated substrate was fabricated and sent to the University of Toronto for examination. Details of their calculations and their preliminary measurements are presented in Appendix A. Appearing in Appendix B is a technical report summarizing additional work at the University of Toronto which was partly supported by this program.

8. CONCLUSIONS

During Year 2, work continued to better understand and improve the MOCVD thin films of CdTe and CdZnTe needed for the mammography imaging arrays. By planarizing the growth susceptor, improved film morphology was realized. Studies of growth rate vs. temperature showed that reasonable growth rates could be obtained at temperatures as low as 250°C using readily-available precursors. Films of CdZnTe were obtained by suitable incorporation of a Zn precursor (dimethyl zinc) into the growth chamber. Electrical characterization of the films continued. Results indicate that the leakage currents are still too high in spite of the use of a CdS/CdTe or CdS/CdZnTe heterostructure. At this point, it is not certain whether the high currents are due primarily to film purity or to grain boundary effects. It is imperative that this problem be solved before the program embarks on deposition of films on active device structures such as TFT arrays. Film improvement will therefore be the primary focus for the coming year.

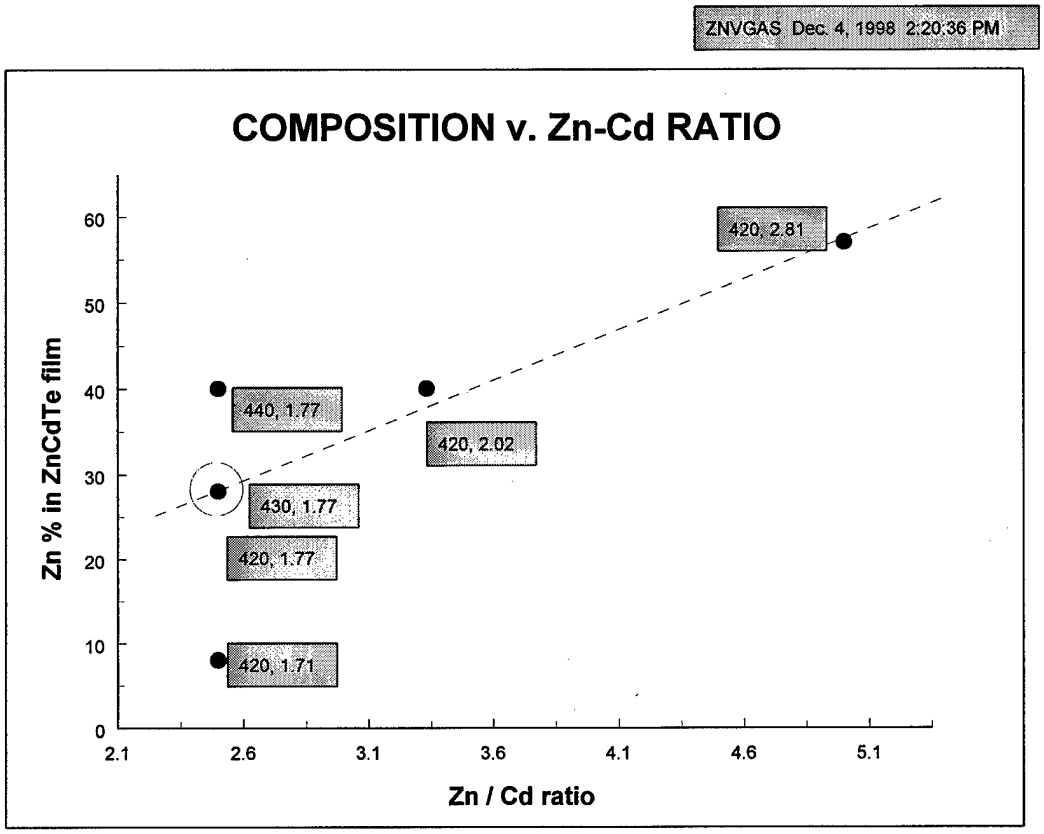

Figure 6 **Experimentally observed dependence of Zn concentration (x) on ratio of Zn-to-Cd flow rates during MOCVD growth in the 420 to 440C temperature range.**

9. REFERENCES

1. M.J. Yaffe, "Digital Mammography," A Categorical Course in Physics; Technical Aspects of Breast Imaging, Edited by A.G. Haus and M.J. Yaffe, 79th Scientific Assembly and Annual Meeting of the Radiological Society of North America; November 28 to December 3, 1993.
2. R.K. Swank, "Absorption and Noise in X-ray Phosphors," *J. Applied Physics* **44**, 4199-4203, (1973).
3. R.M. Nishikawa and M.J. Yaffe, "Signal-to-noise Properties of Mammography Film Screen Systems," *Medical Physics* **12**, 32-39, (1985).
4. F.P. Doty, H.B. Barber, F.L. Augustine, J.F. Butler, B.A. Apotovsky, E.T. Young, and W. Hamilton, "Pixellated CdZnTe Detector Arrays," *Nuclear Instruments and Methods in Physics Research* **A353**, 356 (1994).
5. M. Singh, F.P. Doty, S.J. Friesenhahn, and J.F. Butler, "Feasibility of using CdZnTe Detectors in Electronically Collimated SPECT," *Proceedings of IEEE 1994 Nuclear Science and Medical Imaging Conference* **3**, 1165 (1995).
6. R. Sudharsanan, T. Parodos, Y. Nemirovsky, and N.H. Karam, "CdZnTe Photodiode Arrays for Medical Imaging," presented at the 1995 U.S. Workshop on the Physics and Chemistry of Mercury Cadmium Telluride and Other IR materials, Baltimore, MD, October 10-12 (1995).
7. H.H. Barrett, J.D. Eskin, and H.B. Barber, "Charge Transport in Arrays of Semiconductor Gamma-Ray Detectors," *Physical Review Letters* **75**, 156 (1995).

8. R. Polichar, R. Schirato, and J. Reed, "Development of CdZnTe Energy Selective Arrays for Industrial and Medical Radiation Imaging," *Nuclear Instruments and Methods in Physics Research* **A353**, 349 (1994).
9. S.S. Yoo, S. Sivananthan, J.P. Faurie, B. Rodricks, J. Bai, and P.A. Montano, "New CdTe Photoconductor Array Detector for X-ray Applications," *Appl. Phys. Lett.* **66**, 2037, (1995).
10. M.Cuzin, F. Glasser, J. Lajzerowicz, F. Mathy, and L. Verger, "Applications of CdTe Detectors in X-ray Imaging and Metrology," *Proc. SPIE* **2009**, 192 (1993).
11. Y. Tomita, Y. Hatanaka, T. Taksbayashi, and T. Kawai, "X-ray Imaging Camera Tube Using Sputter-Deposited CdTe/CdS Heterojunction," *IEEE Transactions on Electron Devices* **40**, 315 (1993).
12. D. Shenai-Khatkhate, "Tellurium and Selenium Source Review", Morton International Technical Bulletin #9/90 (1990).
13. R. Korenstein, W.E. Hoke, P.J. Lemonias, K.T. Higa, and D.C. Harris, "Metalorganic growth of HgTe and CdTe at low temperature using diallyltelluride", *J. Appl. Phys.* **62**, 4929 (1987).
14. W.E. Hoke and P.J. Lemonias, "Low-temperature metalorganic growth of CdTe and HgTe films using ditertiarybutyltelluride", *Appl. Phys. Lett.* **48**, 1669 (1986).

APPENDIX A

Estimate of W for Spire CdZnTe

Oct. 11, 1998

Estimate of W for SPIRE CdZnTe

W is the ratio between energy absorbed and charge pairs produced which contribute to current flow. We can estimate W from the current measured in response to x-ray excitation as

$$W = E/n$$

Where E is the energy deposited in a second by the x-ray beam and n is the current expressed in el/s.

Energy deposited on the sample in one second:

$$E = F_{abs}\ X\ A\ E_{ph}\ N$$

where:

$F_{abs} = 0.3$	absorbed fraction of x-rays in 30 micron thick sample
$X = 8$ mR/s	x-ray exposure rate
$A = 0.03$ cm^2	area of sample
$E_{ph} = 30$ KeV	energy of x-ray photons (at 60 kVp)
$N = 2*10^{10}$	number of photons per cm^2 per Roentgen

With these numbers:

$$E = 4.32 * 10^{10}$$

Current

The current obtained under the above conditions is I = 120 pA. Expressed in el/s we have:

$$n = I\ /\ 1.6*10^{-19} = 75 * 10^{7}\ \text{el/s}$$

Calculation of W

$$W = E / n = 4.32 * 10^{10}\ /\ 75 * 10^{7} = 57.6\ \text{eV}$$

N.B. **1.** Thickness of sample roughly estimated from measured capacitance C = 9.5 pF, and active area of sample A = 3 mm^2 . Assuming a dielectric constant $\varepsilon_r = 10.2$ the thickness is given by $t = \varepsilon_0 * \varepsilon_r * A / C$.

2. Field applied across ZnCdTe = 25V / 30 μm

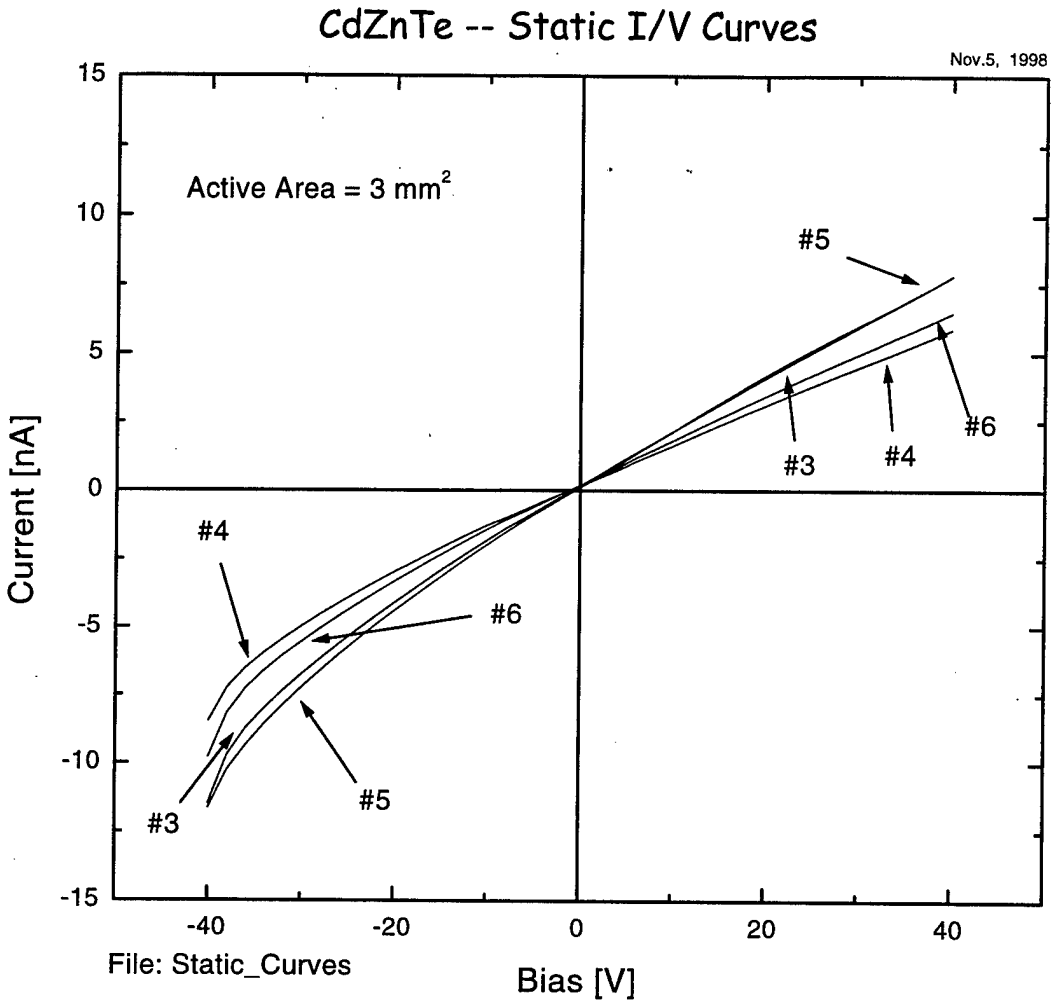
CdZnTe -- Static I/V Curves
Nov.5, 1998
Active Area = 3 mm²
#5
#3
#4
#6
#4
#6
#3
#5
Current [nA]
Bias [V]
File: Static_Curves
15
10
5
0
-5
-10
-15
-40
-20
0
20
40

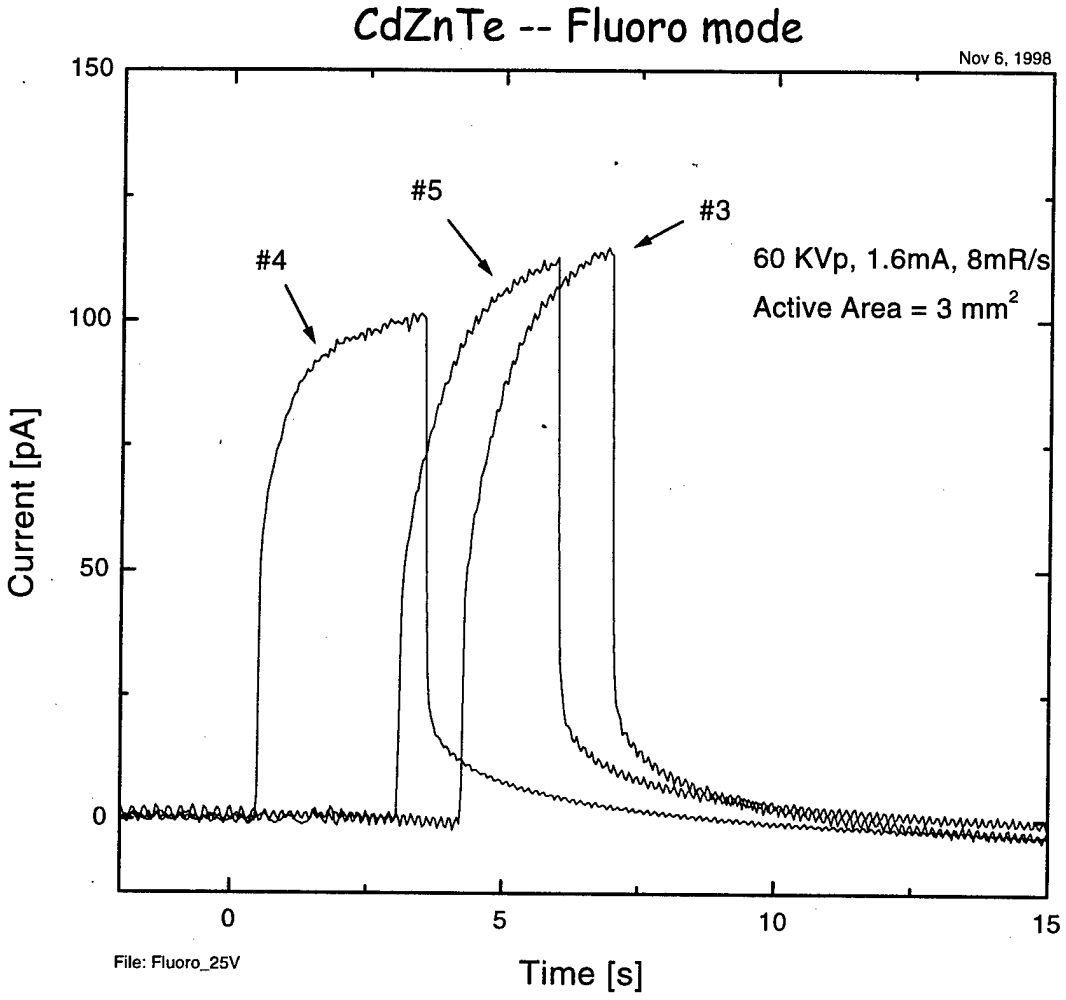
CdZnTe -- Fluoro mode
Nov 6, 1998
150
100
50
0
Current [pA]
#4
#5
#3
60 KVp, 1.6mA, 8mR/s
Active Area = 3 mm2
0
5
10
15
Time [s]
File: Fluoro_25V

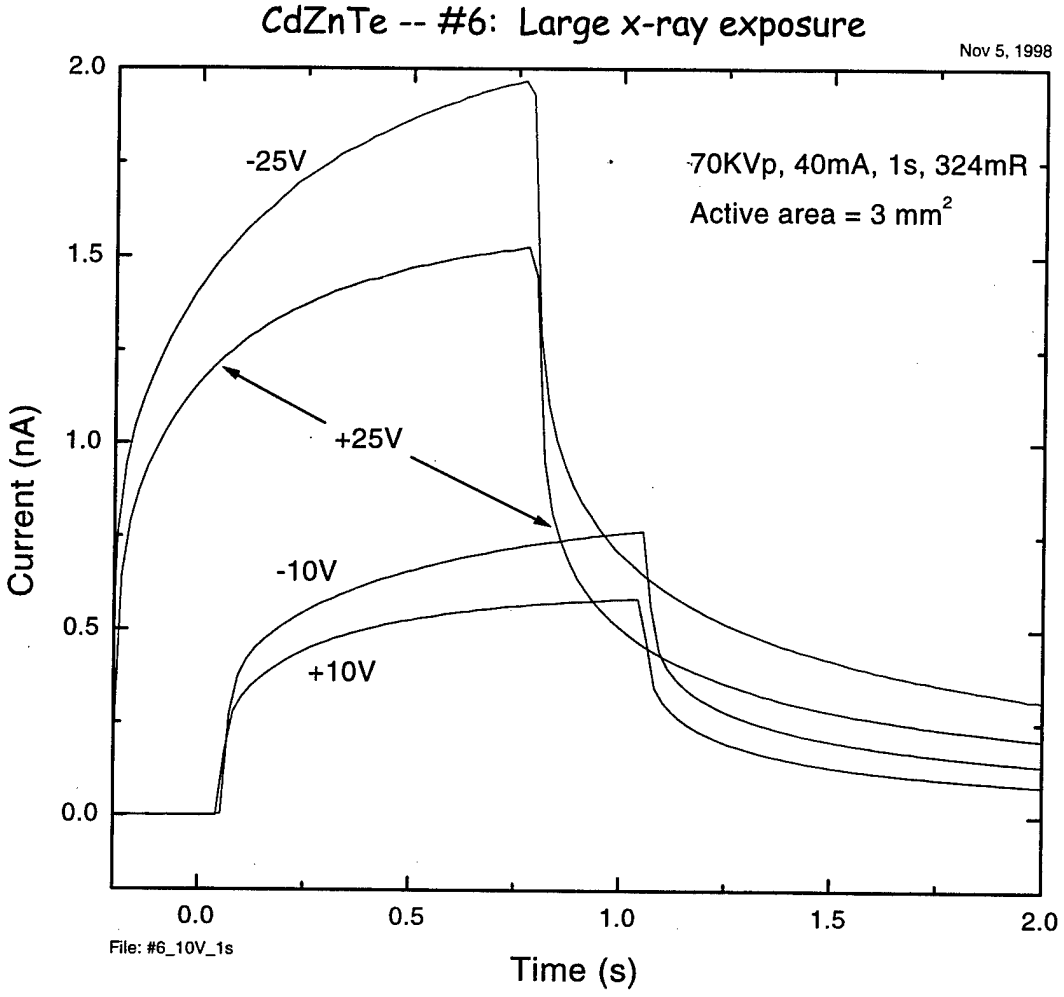
CdZnTe -- #6: Large x-ray exposure
Nov 5, 1998
-25V
+25V
-10V
+10V
70KVp, 40mA, 1s, 324mR
Active area = 3 mm2
Current (nA)
Time (s)
2.0
1.5
1.0
0.5
0.0
0.0
0.5
1.0
1.5
2.0
File: #6_10V_1s

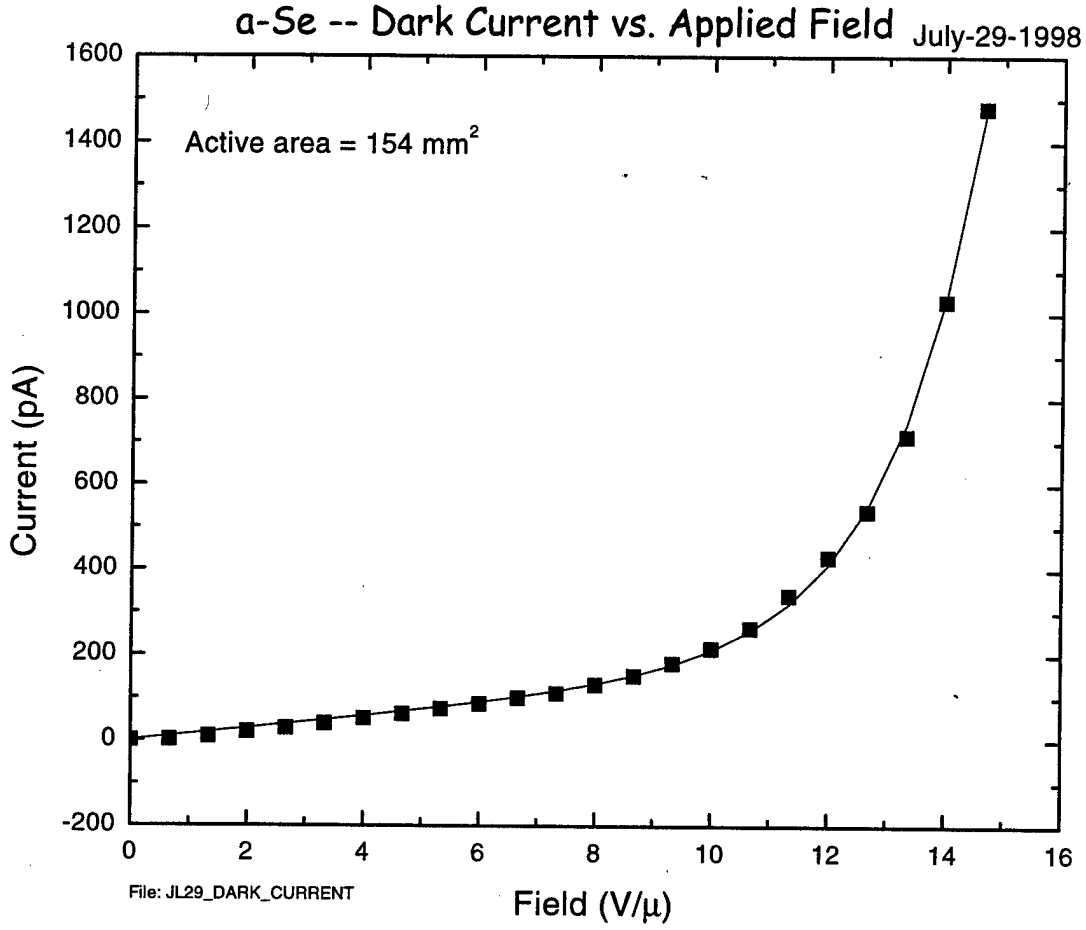
a-Se -- Dark Current vs. Applied Field
July-29-1998
Active area = 154 mm²
Current (pA)
1600
1400
1200
1000
800
600
400
200
0
-200
0
2
4
6
8
10
12
14
16
Field (V/μ)
File: JL29_DARK_CURRENT

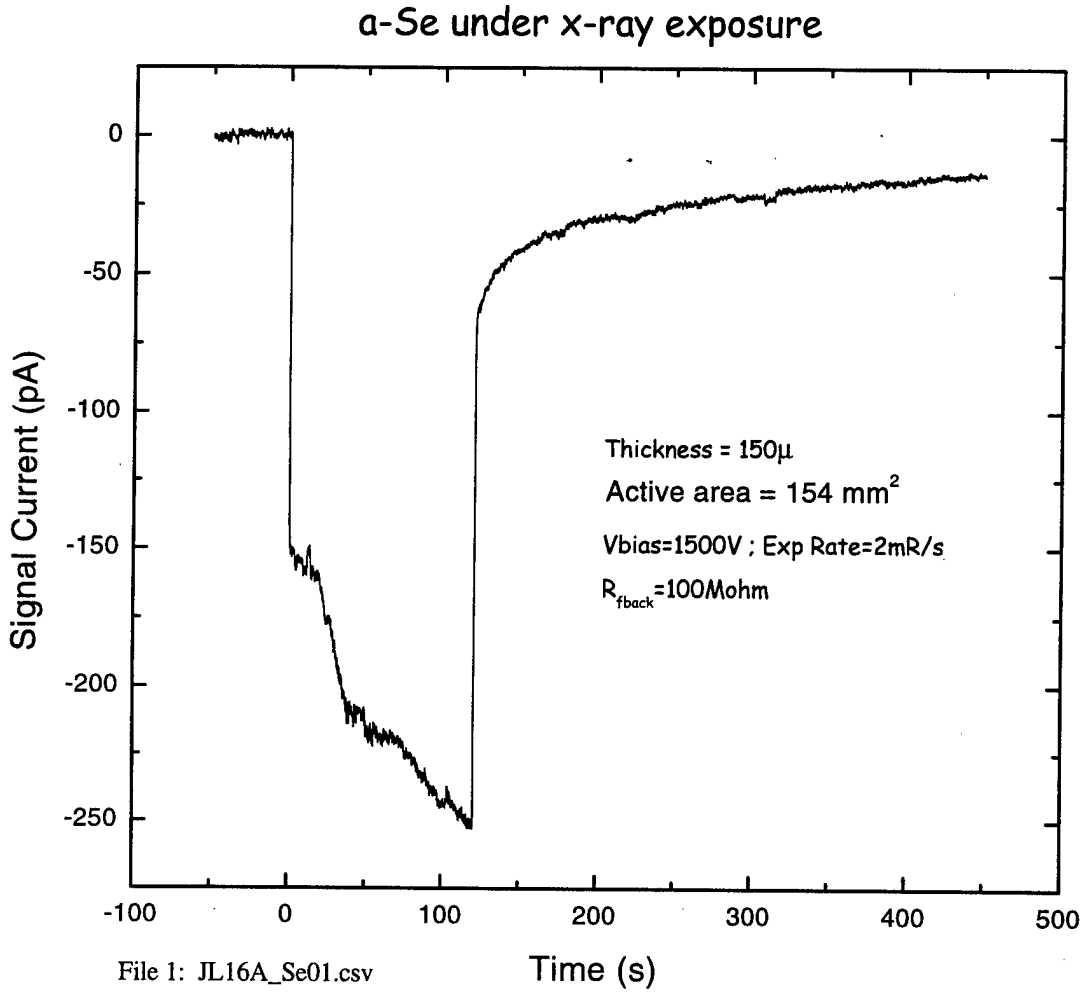

File 1: JL16A_Se01.csv

APPENDIX B

Detective Quantum Efficiency of Direct, Flat Panel X-Ray Imaging Detectors for Medical Applications

Detective Quantum Efficiency of Direct, Flat Panel X-ray Imaging Detectors for Medical Applications

Dylan C. Hunt and J. A. Rowlands
Medical Imaging Research
Sunnybrook and Women's College Health Sciences Centre
University of Toronto
2075 Bayview Avenue
Toronto, M4N 3M5 CANADA

ABSTRACT

Our goal is to develop a large area, flat panel solid-state detector. The detector employs a layer of photoconductor to convert incident x-rays directly to a charge image, which is then read out in real-time using a two dimensional array of thin film transistors (TFTs), or "active matrix". In order to guide the design of an optimum fluoroscopic flat-panel detector, a cascaded linear systems model was developed, from which the spatial frequency dependent detective quantum efficiency (*DQE(f)*) can be obtained. Then *DQE(f)* was calculated as a function of different detector design parameters, *e.g.* pixel fill-factor, x-ray exposure, Swank factor, electronic noise, and the calculation was performed for three different x-ray photoconductors: amorphous selenium (*a*-Se), cadmium zinc telluride (CZT), and lead iodide (PbI_2). A critical comparison was made of the advantages and disadvantages of each photoconductor. The results showed that the *DQE(0)* of all direct detectors has a linear dependence on the pixel fill-factor. For an *a*-Se layer with an electric field of 10 V/μm, *DQE(f)* is significantly degraded by the electronic noise of the detector, especially at very low x-ray exposure rates (*e.g.* 0.1 μR/frame). With CZT and PbI_2, the detector is more tolerant of electronic noise because of the larger number of charge generated for each absorbed x-ray. We have applied our cascaded linear systems model of the direct, flat-panel detector. The theoretical predictions of *DQE(f)* for different detector parameters, *e.g.* the type of x-ray photoconductor, fill-factor, and electronic noise, provide a guideline for an optimum detector design.

Keywords: Amorphous selenium, lead iodide, cadmium zinc telluride, flat panel detector, detective quantum efficiency, imaging, electronic noise, photoconductor.

1. INTRODUCTION

1.1 Flat panel imaging

There has recently been a great deal of interest in digital radiology. Unlike other medical imaging modalities such as CT, ultrasound, or MRI, x-ray imaging remains largely an analog technique. The advantages of digital radiology would be: Co-registration and comparison of x-ray images with images acquired by other means; uncoupled acquisition and display; simplified storage and instantaneous access without requiring locating and transporting film to each viewer; resilience to

damage, and prolonged lifetime and lower loss risk; and finally the possibility of teleradiography where remote locations could be serviced by highly trained personnel at a central hospital or health science centre.

Currently there are two digital x-ray imaging techniques. In one technique a latent image stored in a stimuable phosphor is digitized. The other method is the digitization of the signal from a camera coupled to an x-ray image intensifier. Although the x-ray image intensifier can work at fluoroscopic imaging rates it has several disadvantages: The input phosphor is curved leading to pincushion distortion; veiling glare from scattered x-rays and internal reflection of light; poor resolution due to the coupling of several image conversion stages; susceptibility to magnetic fields leading to "S" distortion, and the intensifier itself is bulky reducing the free movement of the detector, and limiting the viewing angles available. A large area, flat-panel digital x-ray imaging detector has been shown to be a significant improvement over current radiological imaging.

There are two methods for making flat-panel detectors. One method (here referred to as the indirect method) uses a phosphor screen of CsI to convert the x-ray image into a light image that is then converted by an array of *a*-Si:H photo diodes into an electronic image. The complementary method (referred to as the direct method), uses a photoconductor layer to covert the x-ray image directly into an charge image which is subsequently read-out by an active matrix array. The direct method has a higher intrinsic resolution compared to the indirect method because it avoids the x-ray to light conversion stage. Theoretical modeling of an *a*-Se based flat-panel system showed that the system was good for radiography, but indicated difficulties for fluoroscopy, because of low signal, (the average exposure to the detector per frame in fluoroscopy is 1 μR.)

The basic concept of an active matrix readout system for a photoconductor detector is shown in Fig. 1. The active matrix consists of an array of TFT's connected to pixel electrodes and storage capacitors. The TFT's are turned on row by row, and the signal is sent out through the source of the TFT's through separate signal lines. To make the active matrix sensitive to x-rays a photoconductor layer is evaporated onto the panel and voltage is applied through a top electrode. X-rays are absorbed in the photoconductor releasing electrons and holes which drifts towards their respective electrodes under the influence of the applied field, E_{ph}. Once the charge reaches the pixel electrodes it is stored and read out by the active matrix as discussed above.

In order to have good image quality the photoconductor must have several important properties. It must have a large band gap energy, to limit the thermal generation of charge carriers in the bulk. This limits the use of photoconductors for x-ray imaging to those that have a band gap greater than 2 eV. Lead iodide, (PbI_2), cadmium zinc telluride, (CZT), and amorphous selenium, (*a*-Se), are good candidates. The photoconductor should have good bulk charge transport properties, to allow the charge image to reach the pixel electrodes before the charges are lost in traps, and it should have poor surface conductivity to prevent the lateral conduction of the image charge once it has reached the pixels. The photoconductor should be stable under the conditions of use, and over the lifetime of the imaging system. A final important property is a high x-ray to charge conversion efficiency. Recent measurements have shown that the conversion energy of *a*-Se is 42 eV/ehp at 10 V/μm, and

that it can be reduced to 19.2 eV/ehp at 30 V/μm.[1] The conversion energy of PbI_2 and CZT is 5 eV/ehp for both.[2,3] One interesting question that arises is whether 19 eV/ehp is enough to solve the difficulties indicated in fluoroscopy, or if 5 eV/ehp is required. The advantages of *a*-Se are that it has the desired charge transport properties in the bulk and on the surface, it is stable (with the addition of 5% As, and ppm Cl), and it can be made to any desirable size, and up to a thickness of 1 mm.

Single crystal PbI_2 has been used in spectrometers, and deposited PbI_2 has been used in a 1" vidicon for x-ray imaging in real time,[2] and has shown good modulation transfer function, (MTF). Thicknesses of 150 - 250 μm have been reported.[2] Though its high attenuation of x-rays makes it a good candidate, more work needs to be done to increase its size in order to cover a clinically relevant image area, if it is to be used as a direct imaging material.

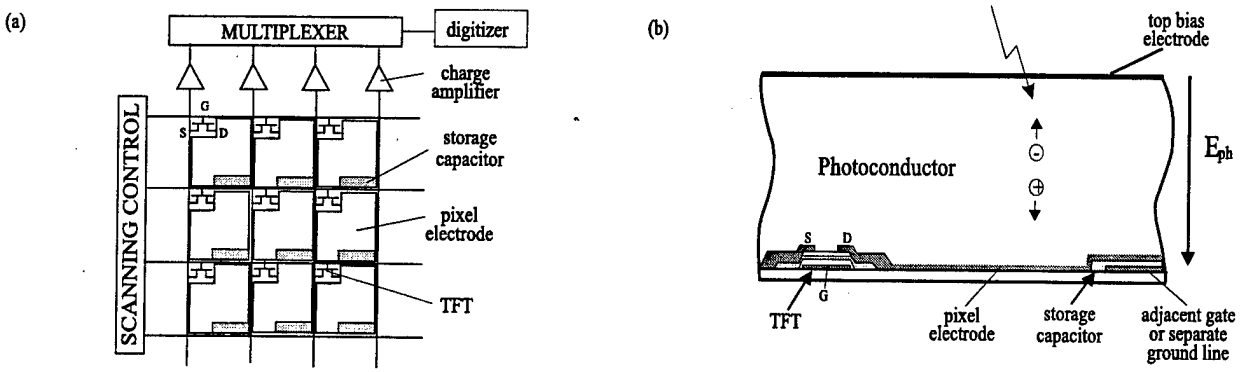

Figure 1. *Basic concept of direct method: (a) a schematic diagram of complete system; (b) a cross section through one pixel.*

Cadmium zinc telluride is a large band gap photoconductor that has been used in devices such as gamma cameras for SPECT imaging.[4] It has also been used in small area direct flat panel imaging systems, which can be operated in real time.[5] CZT is similar to PbI_2 in that it has excellent quantum efficiency, but there is some difficulty in covering a clinically relevant area. Research is also underway to solve the problems of low charge collection efficiency due to the low mobility-lifetime product of the holes and the low fields typically used on this material because of its high dark current.[6,7]

Amorphous selenium is another material that has received a lot of recent attention.[8,9] As mentioned earlier it has the tantalizing virtue that by being amorphous it can be made in any size and almost any thickness. The thickness is limited by the Schubweg. To have sufficient charge collection efficiency the thickness must be less than the Schubweg of each charge carrier. The Schubweg is field dependent, and hence *a*-Se can be made thicker if higher fields are used. At 30 V/μm the hole and electron Schubwegs are S_h = 2 - 20 cm, and S_e = 1 - 9 mm. So a thickness of 1 mm is possible. Further the resistivity of *a*-Se is very high (> 10^{15} Ω-cm) allowing it to support a field as high as 30 V/μm with negligible dark current, and at room temperature. Thus amorphous selenium is the most highly developed photoconductor for x-ray applications.

An experimentally tested theoretical analysis of the frequency dependent detective quantum efficiency (*DQE(f)*)[7] will be used to assess the impact of new measurements of the higher conversion efficiency of *a*-Se on the noise tolerance, and compare with other photoconductors with a conversion energy of 5 eV/ehp.

2. METHOD

2.1 Quantum Efficiency

In order to calculate the detective quantum efficiency for any material it is necessary to know the quantum efficiency as a function of energy. The quantum efficiency can be calculated from knowledge of the linear attenuation coefficient, μ, using the formula,

$$\eta(\varepsilon) = 1 - e^{-\mu(\varepsilon)\tau} \qquad (1)$$

where ε is the energy of the photon, and τ is the thickness of the material in question. The attenuation coefficient of *a*-Se was obtained from standard tables.[10] The attenuation coefficients of PbI_2 and CZT, (here assumed to be $Cd_{0.8}Zn_{0.2}Te$), were calculated from the attenuation coefficients of each material,[10] using the atomic fractions as given in their chemical formulae. Fig. 2 is the resulting plot of the quantum efficiency for each material.

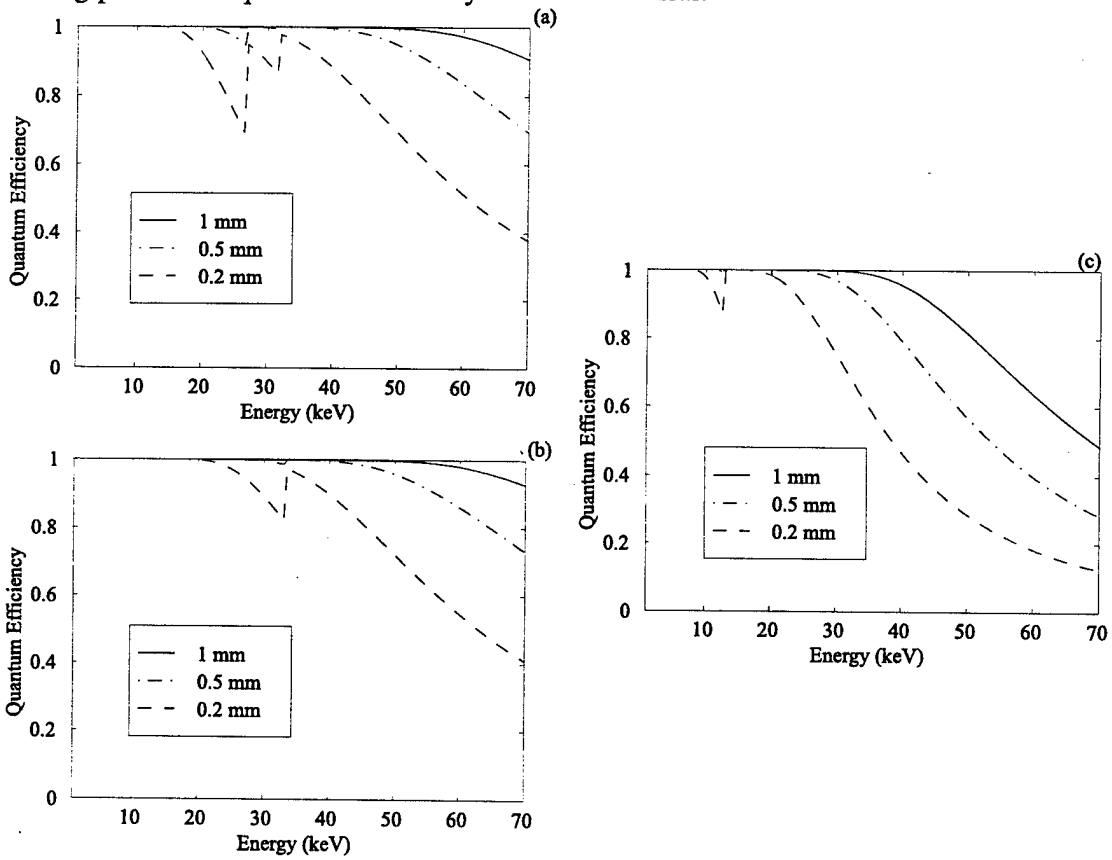

Figure 2. *The quantum efficiency of each photoconductor calculated for various thicknesses. (a) CZT (b) PbI_2 (c) a-Se.*

2.2 The Swank factor

Robert Swank in his paper identified the perturbing effect of varying gain due to fluorescence escape and identified the multiplier, (here called the Swank factor, A_s), that corrected the detective quantum efficiency.[11] For our purposes the Swank factor was determined at each energy by calculating a pulse height spectrum for each material. Poisson noise was assumed, and the only other effect that was included was the introduction of fluorescence escape peaks at the appropriate energies for the materials involved. Compton effects were ignored because the energy was sufficiently low that Compton attenuation was not the main factor. In the compound photoconductors, (PbI_2, and CZT), only fluorescence escape and reabsorption from each individual species in the compound was considered. (The probability that fluorescence from one element would be absorbed by another element, causing that species to fluoresce and then escape is very small.) From a pulse height spectrum the Swank factor is then calculated from the formula,

$$A_s = \frac{M_1}{M_2 M_0} \tag{2}$$

where M_i is the i^{th} moment of the pulse height spectrum.[11] See Fig. 3 for a plot of the Swank factor for each material. These plots are based calculations by Rebecca Fahrig,[12] but where modified to be able to consider other materials including compounds such as CZT and PbI_2. In the case of *a*-Se the calculations were further modified to reflect recently measured data.[13] Note that there is a drop in the Swank factor at the K edge of each element. This contributes to the energy dependence of DQE. There is also a thickness dependence of the Swank factor. As the thickness increases the fluorescence has farther to travel to escape. More of the fluorescence that èscaped from a thin photoconductor is absorbed in a thicker sample.

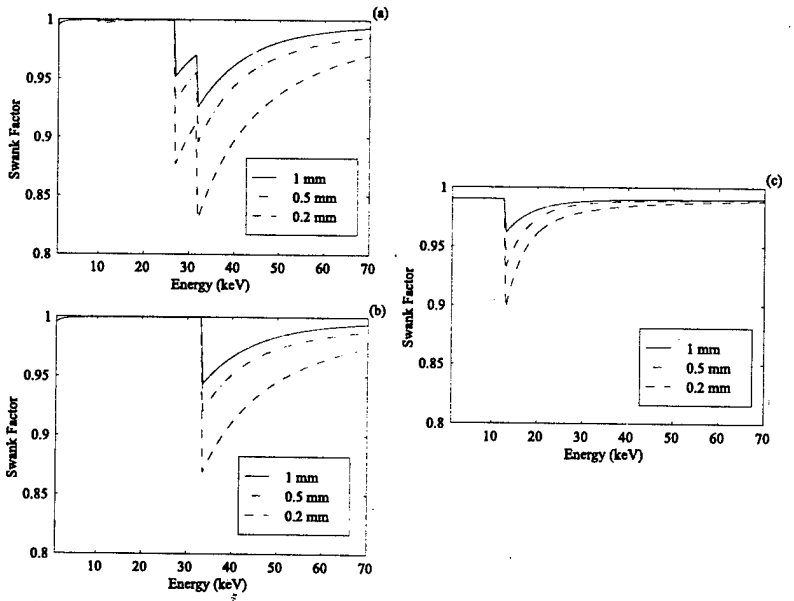

Figure 3. *The Swank factor of each photoconductor calculated at 1, 0.5, and 0.2 mm thicknesses, (a) CZT (b) PbI_2 (c) a-Se.*

2.3 The X-ray Spectrum

Another component needed to for the calculation of the detective quantum efficiency is the incident x-ray spectrum. In fluoroscopy a typical value for the tube voltage is 70 kVp. The spectrum was obtained using Kramers spectrum, and attenuating it by 0.01 mm of tungsten, and then by 2 mm of aluminum. The result is shown in Fig. 4. The spectrum was normalized, and scaled accordingly to match the exposure. With the quantum efficiency, the Swank factor, and the x-ray spectrum the detective quantum efficiency was calculated for CZT, PbI_2, and *a*-Se.

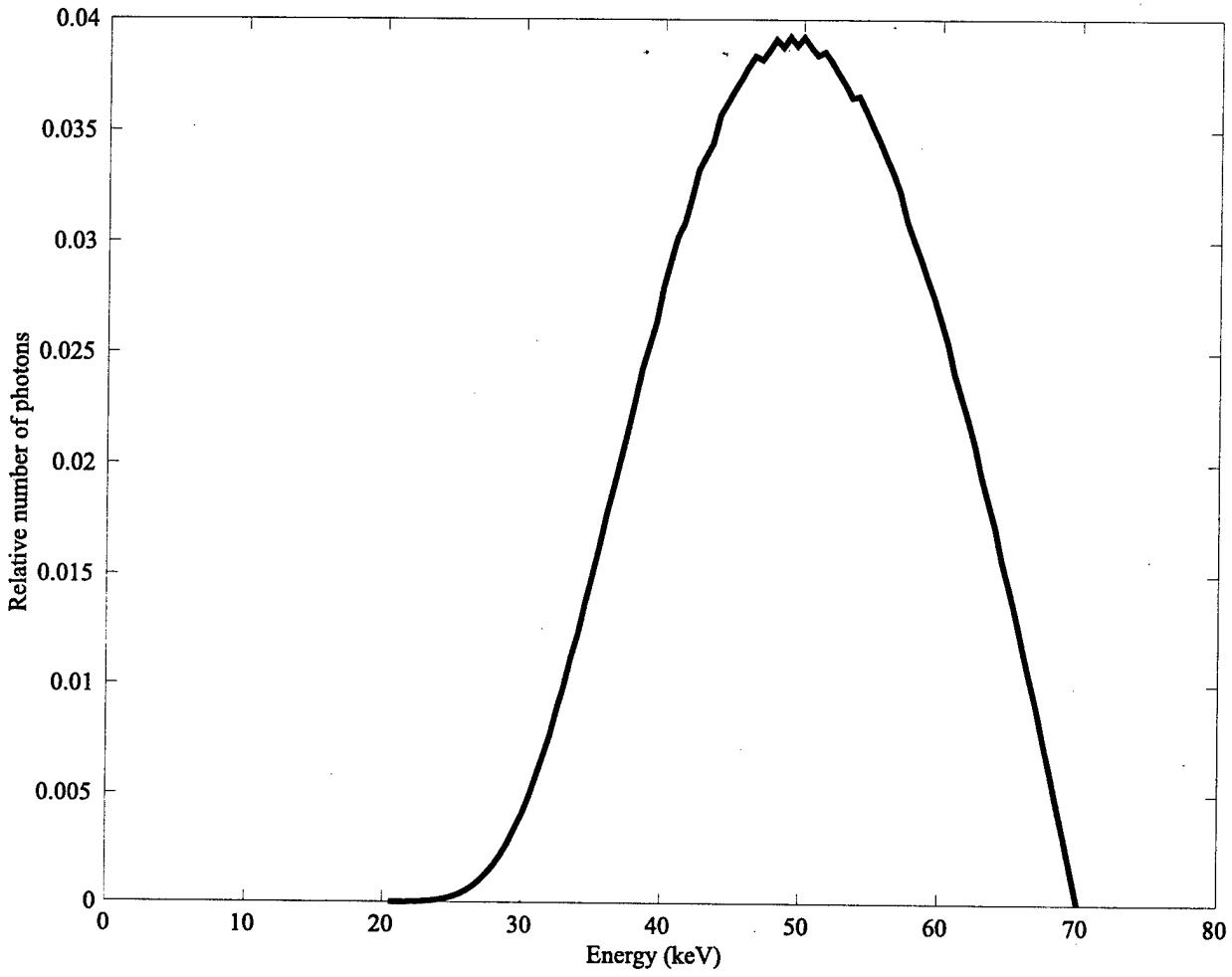

Figure 4. *A graph of the normalized spectrum used in the calculations, (70 kVp, 0.1 mm W, 2 mm Al, and 20 cm of water).*

2.4 The Cascaded Linear Systems Model

To quantitatively compare the performance of each of the three materials the quantity chosen was the detective quantum efficiency, (DQE). The cascaded linear systems model provides a method for calculating the DQE, up to the Nyquist frequency for the flat panel array.[9] The cascaded linear

systems model is discussed in detail in the reference and will only briefly be discussed here.

In the cascaded linear systems model the signal and noise are passed through various stages, such as detection, gain, blurring, addition, and aliasing. At each stage the signal, and noise power spectrum, (NPS), is calculated from the signal, and NPS of the previous stage, and from the characteristics of the current stage. For example, in the case of gain, the new signal is given by, $\Phi_{out} = g\Phi_{in}$, while the NPS is given as, $S_{out} = S_{in}g^2 + \Phi_{in}\sigma_g^2$. In Fig. 5 is a list of the stages considered in this paper. Once the signal and NPS has been calculated for the final stage the detective quantum efficiency can be calculated using the familiar formula $DQE = SNR_{out}^2/SNR_{in}^2$. For the stages given in Fig. 5 this leads to the following formula for the DQE,

$$DQE(\nu) = \frac{a^2}{d^2} \frac{[\int_0^{\varepsilon_{max}} g(\varepsilon)\eta(\varepsilon)\Phi_0(\varepsilon)d\varepsilon]^2 T_m^2(\nu)T_a^2(\nu)}{\overline{\Phi}_0[\int_0^{\varepsilon_{max}} \frac{g^2(\varepsilon)}{A_s(\varepsilon)}\eta(\varepsilon)\Phi_0(\varepsilon)d\varepsilon + S_d(\nu) + \frac{a^2}{d^2}S_a(\nu)]} \quad (3)$$

where, a^2/d^2 is the fill factor, $g(\varepsilon)$ is the gain, $A_s(\varepsilon)$ is the Swank factor, $\eta(\varepsilon)$ is the quantum efficiency, $\Phi_0(\varepsilon)$, is the x-ray spectrum, Φ_0 is the integral of the spectrum, $T_m(\nu)$ is the modulation transfer function of the detector material in question, (assumed in this paper to be unity for all three materials), $T_a(\nu)$ is the modulation transfer function of the flat panel, $S_d(\nu)$ is the NPS of the dark current shot noise, and $S_a(\nu)$ is the NPS of the electronic noise.

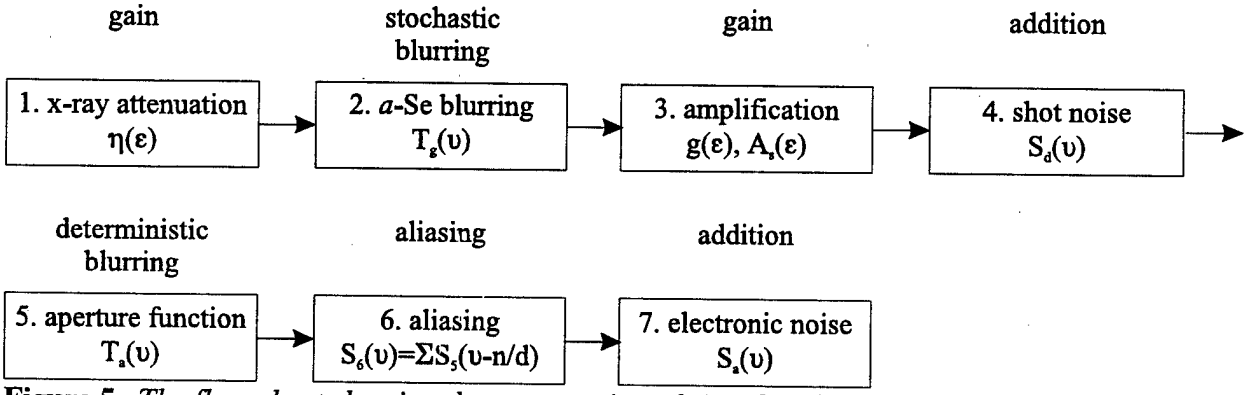

Figure 5. *The flow chart showing the propagation of signal and noise power spectra through the seven detection stages of the self-scanned photoconductor detector.*

2.5 Parameters

The modulation transfer function of the photoconductors, has been set to unity. This is reasonable for CZT, PbI_2, and *a*-Se because the modulation transfer function inherent to these photoconductors

is greater than 0.95 at 2 lp/mm.[2,9] The model is only valid up to the Nyquist frequency of the device, (in this case is 2 lp/mm since the pixels are 250 μm.) The factors considered to differ between photoconductors were: the energy required to create an electron hole pair, ($W_{\pm}$), the quantum efficiency, the Swank factor, and the dark current.

Material	Conversion Efficiency	Resistivity (Ω-cm)	Field (V/μm)	Density (g/cm^3)	Dark Current
CZT	5 eV/ehp	$1.8\text{-}3.3\times10^{10}$	0.1	5.7	10^{-7} Acm^{-2}
PbI_2	5 eV/ehp	5×10^{12}	1.0	6.16	2×10^{-9} Acm^{-2}
a-Se	20 eV/ehp	10^{15}	30	4.26	3×10^{-10} Acm^{-2}

Table 1. The parameters used in the calculation of DQE.

Three parameters of the photoconductors were set to the same value. The thickness of each photoconductors was chosen to be 1 mm. Charge collection efficiencies problems were assumed to be solved, i.e., perfect charge collection efficiency. Third, the fill factor was also assumed to be unity. A fill factor of unity can be achieved either by building a mushroom structure where the pixel electrode sits above the active matrix electronics, or by manipulating the electric field above the pixels through the trapping of charge in the gaps between the pixels. A combination of these two approaches can achieve a fill factor better than 95%.[14]

The dark current for each material was determined from the resistivity as published by various authors,[9,15] (10^{10} Ω-cm for CZT, $5\cdot10^{12}$ Ω-cm for PbI_2, and 10^{15} Ω-cm for *a*-Se), and from the fields required, (0.1 V/μm for CZT, 1 V/μm for PbI_2, and 30 V/μm for *a*-Se). The dark current shot noise was calculated as, $S_d(v) = I_d T_F/e$, where I_d is the dark current, T_F is the time for one frame (T_F = 33 ms in the case of fluoroscopy), and e is the charge of an electron.

Finally, the conversion energy, $W_{\pm}$ was determined from published values, 5 eV/ehp for CZT,[3] 5 eV/ehp for PbI_2,[2] and 20 eV/ehp for *a*-Se.[1] The conversion energy of *a*-Se is known to be a function of the bias field.[16] In this case the bias field was set to a value that would give a conversion energy of 20 eV/ehp, and is 30 V/μm. The values of these parameters, and others are summarized in Table 1. The detective quantum efficiency was determined for a wide range of pixel electronic noise.

3. RESULTS

3.1 Detective quantum efficiency of each photoconductor

Before looking at the performance of the entire imaging system it is instructive to examine the detective quantum efficiency of the photoconductors themselves. Although the quantum efficiency of CZT and PbI_2 is higher than *a*-Se for a given thickness, (as seen in Fig. 2), the Swank factor of *a*-Se is almost unity over the energy range of the spectrum, (which extends from about 15 to 70 keV

as seen in Fig. 4). The drop in the Swank factor occurs at the K edges of each element (whether in a compound or alone). For *a*-Se this drop occurs at ~ 12 keV which is lower than the lowest energy in the spectrum. For CZT, and PbI_2 this drop occurs at the peak of the spectrum where there is the highest number of x-rays. The Swank factor is also a function of the photoconductor's thickness since the probability of fluorescence reabsorption scales with the thickness. The detective quantum efficiency of each photoconductor at a thickness of 1 mm is 0.90 for CZT, 0.91 for PbI_2, and 0.85 for *a*-Se. Despite the high quantum efficiencies of CZT and PbI_2 the integrated detective quantum efficiencies for a 70 kVp spectrum of all three photoconductors are comparable, (a difference of only 6%). The DQE of each photoconductor is further degraded by following stages of the imaging chain.

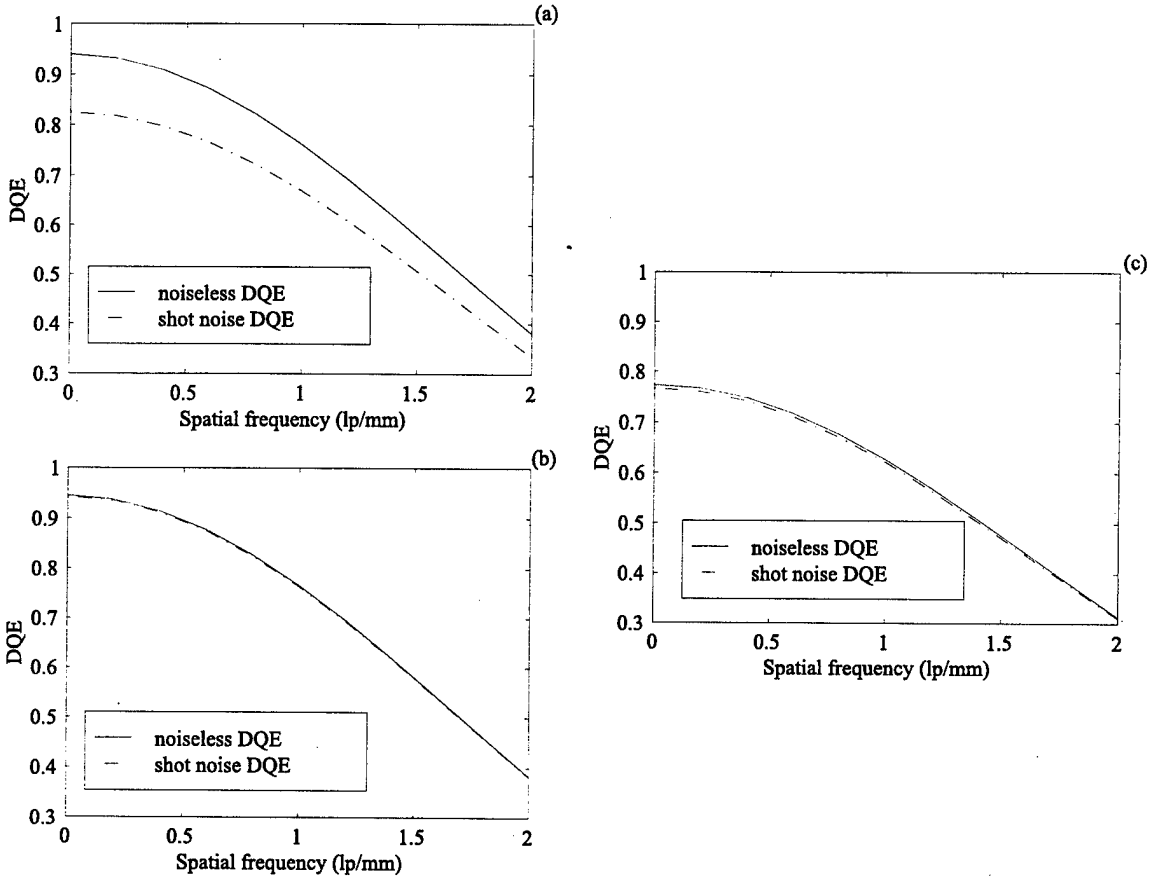

Figure 6. *The detective quantum efficiency without any noise, and with dark current shot noise only. All three sub-figures were calculated with a fill factor of unity, and for the lowest exposure required for fluoroscopy, 0.1 μR/frame, (a) CZT (b) PbI_2 (c) a-Se.*

3.2 The effect of dark current shot noise

The DQE was passed through the stages shown in Fig. 5 except for stage 4 and 7, (addition of shot noise, and electronic noise). Then the addition of shot noise was included in the calculation suing the dark currents in Table 1. The results are plotted in Fig. 6. These calculations were done with a fill factor of unity and at the lowest exposure in fluoroscopy, (0.1 μR/frame). The drop in the DQE

of CZT is perceptible due to the large dark current in CZT. The drop for PbI_2, and *a*-Se is nearly imperceptible because of their high resistivities.

3.3 The effect of electronic noise

The addition of electronic noise occurs after the signal has been integrated on the pixel. It is the last detection stage and is unaffected by sampling or aliasing. The DQE of each material was calculated using the values in table 1 with a fill factor of unity, and for the entire range of exposures used in fluoroscopy, and for a thickness of 1 mm. The results are plotted in Fig. 7 for the lowest exposure, (0.1 μR/frame), as a surface plot of both electronic noise and spatial frequency.

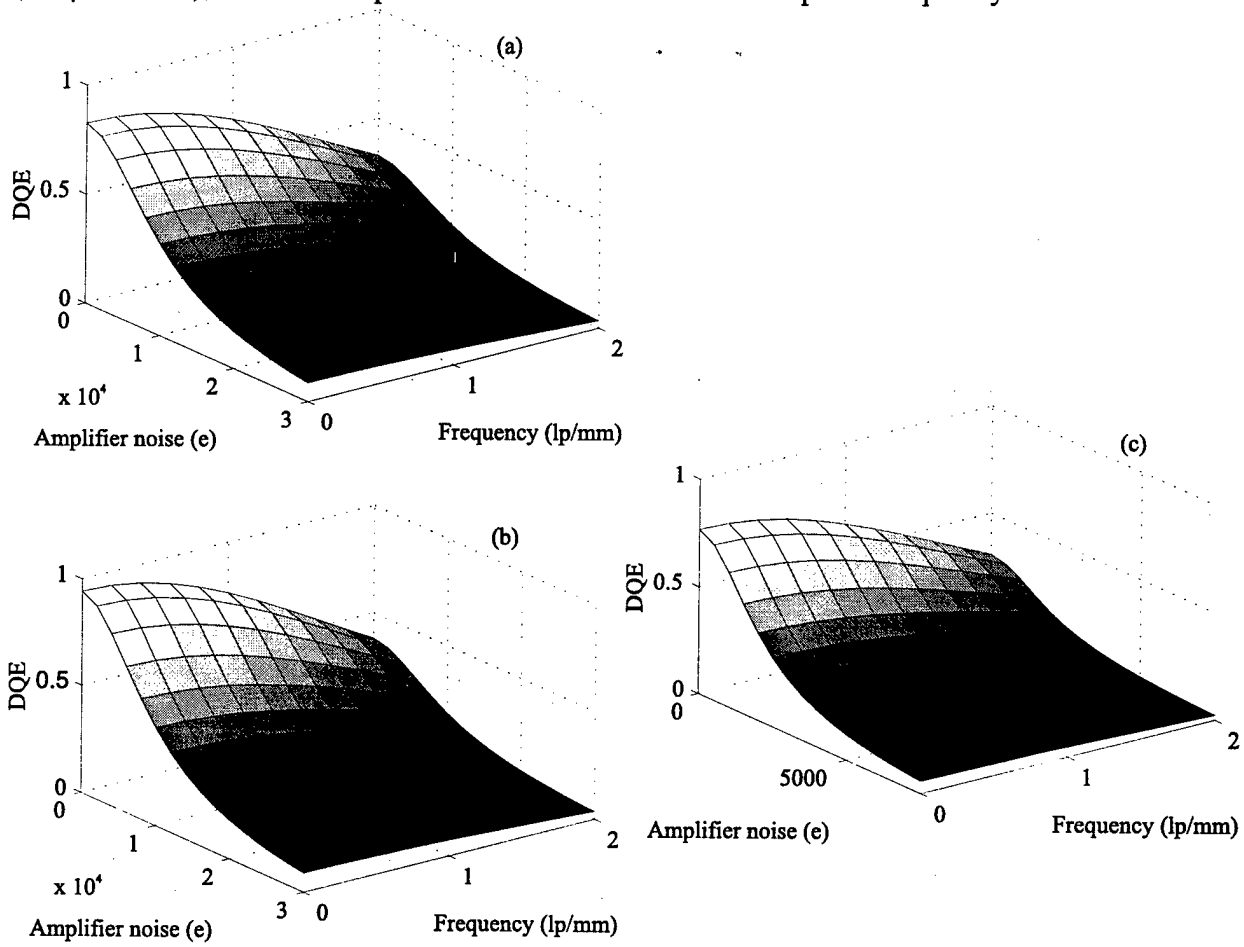

Figure 7. *The surface plot of DQE as a function of amplifier noise, and spatial frequency, at the lowest exposure needed for fluoroscopy (0.1 μR/frame). The dark current shot noise was included in the calculation, hence the DQE without electronic noise corresponds to the dashed plots in Fig. 6. (a) CZT (b) PbI_2 (c) a-Se.*

4. DISCUSSION

Because there is aliasing in this system the DQE follows the square of the MTF of the system, up to the Nyquist frequency. The effect of aliasing is to fold back noise from spatial frequencies above the Nyquist frequency. This makes an otherwise well behaved NPS white so that it no longer

follows the MTF of the system. Since it was assumed that the MTF of the photoconductors were unity, the DQE follows the square of the aperture function. This drop in DQE is a function of the pixel size and is independent of the photoconductor. This method for dealing with aliasing provides an unambiguous description of the detector properties up to the Nyquist frequency.

As a function of electronic noise the DQE drops, but this drop is preventable. As shown in Fig. 7 the drop for *a*-Se is more severe and shows that *a*-Se is less tolerant of electronic noise than PbI_2 and CZT. The main factor which determines noise tolerance is the conversion efficiency. The materials with the higher conversion efficiencies, (i.e. lower $W_{\pm}$) will have their DQE drop off more slowly as a function of electronic noise. Close inspection of the behavior of the DQE in Fig. 7 will reveal that the drop is almost directly proportional to the conversion efficiency. The DQE of *a*-Se has dropped to half its initial value at 1900 electrons per pixel where the value is 7900 electrons per pixel for CZT and PbI_2. A factor of 4, exactly the same factor difference between 5 eV/ehp and 20 eV/ehp.

The conversion energy in *a*-Se is a function of the electric field. Our most recent measurements show that at 30 V/μm, $W_{\pm}$ = 19.2 eV/ehp, 2.6 times better than 50 eV/ehp, (the commonly quoted value), and 2.2 times better than 42.3 eV/ehp, (our measured value at 10 V/μm). The value for $W_{\pm}$ continues to drop at higher fields. Amplifier noise levels of 1000 *e* are obtainable with current technology. Operating *a*-Se at 30 V/μm to get a $W_{\pm}$ of 19.2 eV is sufficient to become quantum noise limited with the current system. If more noise tolerance is desired then either increasing the field of *a*-Se or switching to CZT or PbI_2 would be required.

5. CONCLUSIONS

The calculation of DQE was performed for three direct photoconductor materials: CZT, PbI_2, and *a*-Se. The single most important factor in determining noise tolerance in direct imaging photoconductors was shown to be the conversion energy. The DQE drops off at low exposure rates as a function of electronic noise at a rate which is proportional to the conversion efficiency. Provided the photoconductors can all be made at thicknesses, sizes, fill factors, and collection efficiencies assumed in the above calculations, and that *a*-Se can be operated at fields that reduce its conversion energy, then for flat panel direct x-ray fluoroscopic imaging any of these photoconductor can be used, though for the best performance PbI_2 is the best choice. The drop in DQE as a function of spatial frequency cannot be avoided since it is due to aliasing and is thus independent of the choice of photoconductor.

ACKNOWLEDGMENTS

This work is financially supported by the National Cancer Institute of Canada (NCIC) through a Terry Fox Program Project Grant "Imaging for Cancer" and by the Natural Sciences and Engineering Research Council of Canada through a University Industry CRD grant also supported by Litton Systems Canada and Noranda Advanced Materials and a US Army Mammography Grant held by

SPIRE Corporation. The authors would like to warmly acknowledge helpful discussions with James Mainprize and Dr. Ira Blevis.

REFERENCES

1. I. M. Blevis, D. C. Hunt, J. A. Rowlands. "Digital radiology using amorphous selenium and active matrix flat panel readout: Photoconductive gain and gain fluctuations." SPIE, (these proceedings in press).

2. K. S. Shah, P. Bennett, M. Klugerman, L. P. Moy, G. Entine, D. Ouimette, and R. Aikens. Lead Iodide Films for X-ray Imaging. SPIE **3032**, 395. (1997)

3. A. Niemelä, and H. Sipilä. "Evaluation of CdZnTe Detectors for Soft X-Ray Applications." IEEE Trans. Nucl. Sci. **41**, 1054. (1994)

4. H. B. Barber, H. H. Barrett, and F. L. Augustine. "Development of a 64×64 CdZnTe array and associated readout integrated circuit for use in nuclear medicine." Journal of Electronic Materials, **26**, 765. (1997)

5. R. Sudharsanan, T. Parodos, A. Ruzin, Y. Nemirovsky, and N. H. Karam. "CdZnTe Photodiode Arrays for Medical Imaging". Journal of Electronic Materials, **25**, 1318. (1996)

6. J. D. Eskin, H. H. Barrett, H. B. Barber, and J. M. Woolfenden. "The Effect of Pixel Geometry on Spatial and Spectral Resolution in CdZnTe Imaging Array." (To be published.)

7. J. D. Eskin, H. B. Barber, and H. H. Barrett. "Variations in pulse-height spectrum and pulse timing in CdZnTe pixel array detectors." SPIE **2859**, 46. (1996)

8. W. Zhao, I. Blevis, S. Germann, D. Waechter, Z. Huang, and J. A. Rowlands. "Digital Radiology Using Active Matrix Readout of Amorphous Selenium: Construction and Evaluation of a Prototype Real-Time Detector." Med. Phys. **24**, 1834. (1997)

9. W. Zhao, and J. A. Rowlands. "Digital Radiology Using Active Matrix Readout of Amorphous Selenium: Theoretical Analysis of Detective Quantum Efficiency." Med. Phys. **24**, 1819. (1997)

10. E. F. Plechaty, D. E. Cullen, F. J. Howerton: Tables and graphs of photon interaction cross sections from 1.0 keV to 100 MeV derived from LLL evaluated nuclear data library. UCRL-50400 vol. 6 revision 1. University of California, Lawrence Livermore Laboratory, 1975. Springfield, Va; National Technical Information Service, 1975.

11. Robert K. Swank. "Absorption and noise in x-ray phosphors." J. Appl. Phys., **44**, 4199. (1973)

12. Rebecca Fahrig, J. A. Rowlands, and Martin J. Yaffe. "X-ray imaging with amorphous selenium: Detective quantum efficiency of photoconductive receptors for digital mammography." Med. Phys. **22**, 153. (1995)

13. I. M. Blevis, D. C. Hunt, and J. A. Rowlands. "X-ray imaging using amorphous selenium: Determination of Swank factor by pulse height spectroscopy." Med. Phys. in press.

14. G. Pang and J. A. Rowlands. "Digital radiology using active matrix readout of amorphous selenium: Geometrical and effective fill factors." (submitted to Medical Physics)

15. Y. Nemirovsky, A. Ruzin, and G. Asa. "Study of the Charge Collection Efficiency of CdZnTe Radiation Detectors." Journal of Electronic materials, **25**, 1221. (1996)

16. J. A. Rowlands, G. DeCrescenzo, and N. Araj. "X-ray imaging using amorphous selenium: Determination of x-ray sensitivity by pulse height spectroscopy." Med. Phys. **19**, 1065. (1992)